Available online at www.sciencedirect.com
ScienceDirect
Journal of Power Sources 168 (2007) 513–521
JOURNAL OF POWER SOURCES
www.elsevier.com/locate/jpowsour

Evaluation of the effects of oxygen evolution on the capacity and cycle life of nickel hydroxide electrode materials

Graeme A. Snook [1], Noel W. Duffy, Anthony G. Pandolfo *

CSIRO-Energy Technology, Bayview Avenue, Clayton, Victoria 3168, Australia

Received 8 November 2006; accepted 1 February 2007
Available online 1 March 2007

Abstract

The effect of charge–discharge cycling on the capacity of surface-adhered nickel hydroxide ($Ni(OH)_2$) micro-particles is investigated in aqueous KOH by cyclic voltammetry, and compared with that for pasted nickel hydroxide electrodes. Cyclic voltammetry on adhered $Ni(OH)_2$ micro-particles enables rapid screening of four types of commercially available, battery-grade, nickel hydroxide samples and allows the separation of the oxidation process from the oxygen evolution reaction. With large pasted electrodes, due to their high uncompensated resistance (R_u), these processes are poorly resolved. Pasted β-nickel hydroxide electrodes with a specific capacity of between 190 and 210 mAh g^{-1} are charged and discharged at constant currents greater than 15 C (18 mA cm^{-2}). With no voltage limit in the charging profile, excess oxygen evolution occurs and capacity fading is observed within the first 50 cycles. Loss of capacity is attributed to the degradation of the electrode due to excess oxygen evolution at switching potentials greater than 0.55 V versus Hg/HgO (1 M KOH). X-ray diffraction (XRD) measurements confirm the formation of γ-NiOOH in these electrodes. Limiting the cell voltage to 1.5 V, and thereby minimizing oxygen evolution, results in no observed capacity loss within 100 cycles, and only β-$Ni(OH)_2$ can be detected by XRD phase analysis.

Keywords: Nickel hydroxide; Solid micro-particles; Pasted electrodes; Dopants; Battery cycle-life; Oxygen evolution

1. Introduction

Nickel hydroxide ($Ni(OH)_2$) has been widely used as the positive electrode material in nickel-based secondary batteries [1]. Good cycleability, high specific power and specific energy of these electrodes makes Ni-Cd and Ni-MH batteries ideally suited to a wide range of consumer applications that include power tools and hybrid electric vehicles. At high discharge rates (power) or elevated temperatures, however, the capacity of $Ni(OH)_2$ batteries is adversely affected and can result in capacity fading, increased internal resistance [2] and decreased cycle-life [1].

The extended or long life performance of these batteries is often limited by the efficiency of the positive electrode that, in alkaline media, is governed by the oxidation of nickel hydroxide and the reduction of nickel oxy-hydroxide ($Ni(OH)_2 + OH^- \leftrightarrow NiOOH + H_2O + e^-$) [3–9]). The $Ni(OH)_2$/NiOOH charge–discharge process is believed to be a solid-state, proton intercalation/de-intercalation reaction, whereby both electrons and protons are exchanged and the processes are considered to be controlled by the bulk solid diffusion of protons [10,11]. The accepted scheme for the $Ni(OH)_2$/NiOOH couple involves more than one phase and can be summarized as [12]:

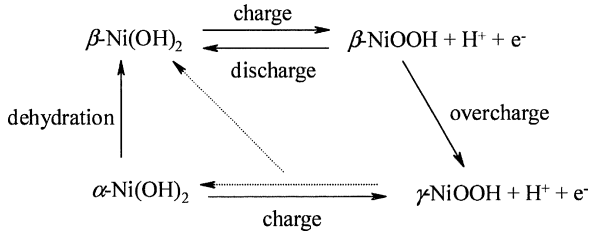

The turbostratic α-phase is initially formed during the chemical synthesis of nickel hydroxide and is transformed (dehydrated) to the more thermodynamically stable β-phase, by ageing in KOH [13]. β-$Ni(OH)_2$ has a well-defined crys-

* Corresponding author.
E-mail address: tony.pandolfo@csiro.au (A.G. Pandolfo).
[1] Present address: CSIRO-Minerals, Box 312, Clayton South, Victoria 3169, Australia.

0378-7753/$ – see front matter.
doi:10.1016/j.jpowsour.2007.02.060

talline structure and is the active material in chemically-prepared nickel battery electrodes. In batteries, charging of the nickel hydroxide electrode involves the homogenous solid-state oxidation of β-$Ni(OH)_2$ to β-NiOOH. Overcharging of β-$Ni(OH)_2$ can, however, lead to the formation of γ-NiOOH with a subsequent swelling of the positive electrode (interlayer spacing changes from 4.7 to 7 Å), which enables the intercalation of water molecules and cations and thereby causes a rapid deterioration of capacity on cycling [14,15].

The charge process of the $Ni(OH)_2$ electrode usually occurs in competition with an oxygen evolution reaction (OER) that is due to the accompanying oxidation of hydroxide ions ($4OH^- \rightarrow O_2 + H_2O + 4e^-$). The mechanism of the oxygen evolution is substrate dependant [16,17] and the degree of oxygen evolution increases when cycling nickel hydroxide electrodes to more extreme potentials [4–7,14,16,18–30]. To ensure maximum capacity, nickel hydroxide electrodes are often cycled to slight overpotentials so that some oxygen evolution on charging is generally unavoidable, particularly at high temperatures at which the OER occurs at a lower voltage [1]. Therefore, a balance needs to be achieved between the charging of $Ni(OH)_2$ and the oxygen evolution reaction (OER). This balance is complicated by the overlap that exists between the potential range at which the charging of the $Ni(OH)_2$ takes place and the potentials at which the OER and undesirable phase changes begin to occur.

Effective charging of the $Ni(OH)_2$ electrode to obtain maximum capacity also depends on particle size, morphology, additives and electrode preparation. In particular, additives such as aluminium, chromium and manganese have been reported [4–7,14,16,20–30] to affect the relative potentials of nickel hydroxide oxidation and oxygen evolution [19], whilst other additives, such as iron, are detrimental to the performance of nickel hydroxide due to catalyzing of the oxygen evolution reaction [29,30]. Additives such as aluminium can stabilize the α-phase of nickel hydroxide [4,26,31], whereas additives such as Ni, Co, CoO, $Co(OH)_2$, ZnO and $Cd(OH)_2$ increase the electron conductivity, the oxygen evolution potential and active material utilization [32]. It should be noted that additives that increase the conductivity will also shift the oxidation peak potential of the nickel hydroxide due to a subsequent reduction in the ohmic drop [33], a distortion that we have noted in the work of other authors [23].

The primary focus of the present work is to determine the $Ni(OH)_2$ oxidation/reduction potentials and the OER onset potentials for a range of $Ni(OH)_2$ samples, to identify beneficial additives, and to define strategies to improve the performance and cycle-life of nickel hydroxide electrodes. Two voltammetric techniques are used to monitor and investigate the charging of $Ni(OH)_2$ electrode materials. It is demonstrated that cyclic voltammetry (CV) on an array of nickel hydroxide micro-particles, attached to a glassy carbon (GC) electrode, allows accurate measurement of the relative potentials of nickel hydroxide oxidation (charging) and the onset of oxygen evolution. Whilst this simple procedure has been used elsewhere [34–36], the technique of abrasively attaching nickel hydroxide micro-particles to an electrode has not been widely applied to investigate the behaviour of nickel hydroxide in battery applications or in battery research in general [37]. These results are compared with galvanostatic charge–discharge cycling results (incorporating electrode potential monitoring) from larger pasted nickel hydroxide electrodes.

2. Experimental

Battery-grade nickel hydroxide samples were obtained directly from commercial suppliers and used as-received. The physical and chemical properties of the samples are listed in Table 1. Freshly prepared 7 M KOH (AR grade, Ajax Chemicals) served as the electrolyte in all experiments.

The $Ni(OH)_2$-adhered glassy carbon electrodes (3 mm diameter, BAS) were prepared by abrasively attaching the $Ni(OH)_2$ particles to their surfaces. A glassy carbon electrode was selected as a suitable substrate since the oxygen evolution potential occurs at a greater potential (∼150–200 mV more positive) on the bare surface than on the surface-adhered nickel hydroxide. Cyclic voltammetry experiments were repeated multiple times to achieve comparable currents by varying the amount of attached solid. Electrode surfaces were cleaned, polished and rinsed between each experiment. Cyclic voltammetric measurements were performed using a VoltaLab PST050 (Radiometer) in a three-electrode configuration with a platinum mesh counter electrode in a separate compartment. A Hg/HgO (1 M KOH) reference electrode with a Luggin capillary was positioned as close to the working electrode as possible to minimize the ohmic drop. The typical scan rate was 20 mV s^{-1}, with a range from 2 to 100 mV s^{-1}.

Pasted electrodes were prepared by mixing nickel hydroxide, conductive graphite flakes (Timcal) and PTFE binder (Aldrich, 60% dispersion in water) with sufficient water to form a free-flowing paste. The paste was coated on a 0.3-mm thick nickel foil collector (typically 5 cm × 5 cm), using a grooved rod applicator. After overnight drying at 35 °C, the electrode coating was compacted by light rolling, before ageing in KOH for at least 1 h prior to assembly or testing.

Cyclic voltammetry of the pasted $Ni(OH)_2$ electrodes was carried out by means of a Solartron 1470 analyser. A scan rate of 5 mV s^{-1} was necessary to minimize the peak current (I_p) within the measurement range of the instrumentation (typically giving $I_p < 2$ A). An oversized, metal-hydride, counter electrode was used to ensure that the cell response was limited by the capacity of the nickel hydroxide electrode. The two electrodes were separated by a 150-μm alkaline battery separator (Japan Vilene

Table 1
Physical and chemical properties of different types of battery-grade nickel hydroxide samples

$Ni(OH)_2$ sample code	Cobalt coated	FWHM (101) (°2Theta)	Particle size (μm)	Analysis (%w/w)			
				Ni	Co	Zn	Cd
Type A	Y	0.99	9.1	58.4	5.4	3.5	<0.01
Type B	Y	1.05	12.6	59.2	4.2	<0.01	3.4
Type C	Y	1.15	11.7	58.4	5.1	3.5	<0.01
Type D	N	1.18	10.3	57.2	1.5	3.8	<0.01

Co. Ltd.) and held under moderate pressure (approx. 360 kPa) in a flooded-electrolyte, screw-type, compression cell. A Hg/HgO (1 M KOH) reference electrode was positioned as close to the electrode pair as possible.

Potential monitoring during charge–discharge cycling was undertaken with a purpose-built, computer controlled, in-house instrument interfaced to a data-acquisition system. Unless stated otherwise, the current used for charge and discharge was 400 mA (equivalent to 18 mA cm^{-2}).

Samples for analysis by scanning electron microscopy (SEM) were mounted in epoxy, cross-sectioned and coated with carbon using a Dynavac CS300 sputter coater. Images of the samples were obtained with a Philips XL30 field emission scanning electron microscope (FESEM) that had an accelerating voltage of 20 kV. Energy dispersive spectroscopy (EDS) studies were performed with LinkISIS equipment (Oxford Instruments Pty. Ltd.).

X-ray diffraction (XRD) phase analysis of samples was performed on either a Philips X'Pert Powder Diffractometer or a PANalytical Horizontal X'Pert PRO Multi-Purpose Diffractometer (MPD) using copper Kα radiation and tube settings of 40 kV and 40 mA.

3. Results and discussion

Previous measurements [22,38–40] of the properties of a single micro-particle of nickel hydroxide between two gold microelectrodes found little direct comparison with the behaviour that is generally shown by pasted nickel hydroxide battery electrodes. This is largely due to minimal contact between the electrodes and the particle. The study reported here demonstrates that an array of micro-particles of nickel hydroxide attached to a glassy carbon electrode provides better contact to the particles and enables the potential of the OER on nickel hydroxide to be determined by cyclic voltammetry. This technique offers advantages in terms of simplicity and ease of experimental utilization which, in turn, allows rapid screening of electrode materials.

Since the technique employs a small amount of active material (micrograms), firmly embedded into the electrode, the distortions that arise from 'ohmic drop' are greatly reduced due to lower currents (I) and the less resistive pathways (R_u) that now exist at the edges of the crystals. By contrast, the large ohmic drop (IR_u), typically associated with pasted electrodes, will not only result in a significant shift of the nickel hydroxide oxidation and OER peaks but also the relative position and magnitude of each peak will shift by differing amounts (due to IR_u effects) and result in large errors.

3.1. Cyclic voltammetry of nickel hydroxide particles attached to glassy carbon

3.1.1. Effect of oxygen evolution reaction on capacity of nickel hydroxide

Cyclic voltammograms for cobalt-coated $Ni(OH)_2$ particles (Type A, see Table 1 for $Ni(OH)_2$ properties) abrasively attached to a glassy carbon (GC) electrode are shown in Fig. 1. During the first 10 cycles, using a rather large voltage window (0–650 mV), the peak current (I_{ox}^{P}) at ~0.4 V, corresponding to the oxidation of nickel hydroxide, increases with each cycle up to a value of 85 μA on the 10th cycle (Fig. 1(a)). The OER is seen as a sharp rise in current at potentials >550 mV and results in gas evolution from the electrode surface. It is noteworthy that neither the shape of the nickel hydroxide process nor the magnitude of the background current changes during these cycles, which indicates an increase in active material utilization. Similar increases in capacity, upon initial cycling, have been reported with battery-type nickel hydroxide electrodes and the process is usually referred to as 'conditioning' or 'formation' [3,41].

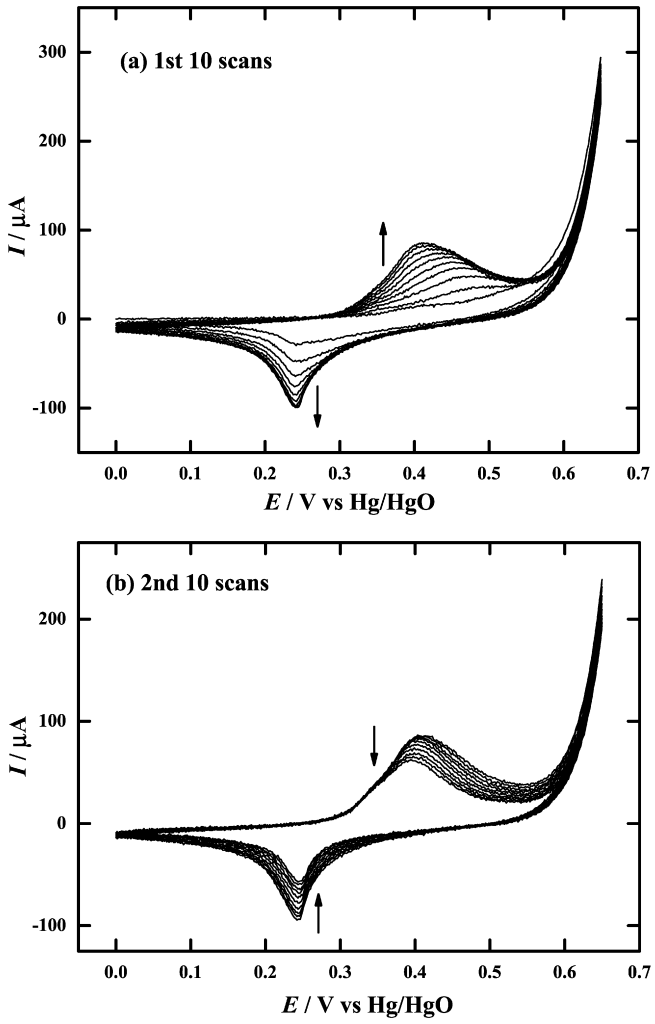

Fig. 1. Cyclic voltammogram of solid cobalt-coated $Ni(OH)_2$ particles (Type A) adhered to a glassy carbon electrode obtained at scan rate of 20 mV s^{-1} with a switching potential (E_{sw}) of 650 mV. (a) First 10 cycles; (b) second 10 cycles. (Arrows indicate increasing or decreasing currents with each successive scan.)

The same electrode was then cycled for an additional 10 cycles whereby the peak current associated with the nickel hydroxide oxidation process (I_{ox}^{P}) now begins to decrease with each successive scan, and hence its capacity diminishes (Fig. 1(b)). The OER current remains relatively unchanged. It is apparent that the evolution of oxygen strongly affects both the performance and the life of the nickel hydroxide electrode. It is

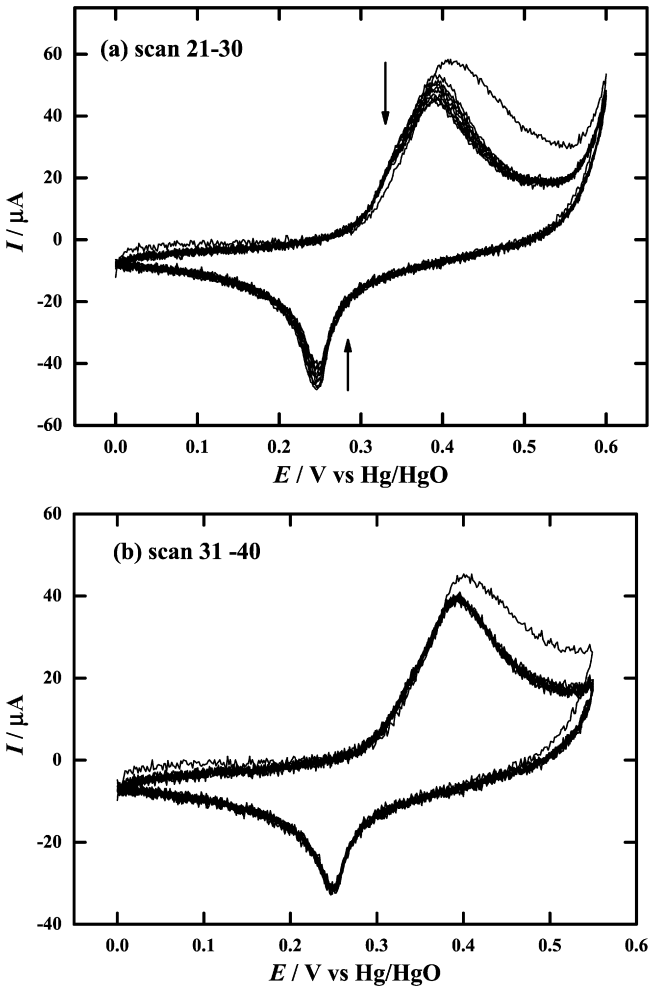

Fig. 2. Cyclic voltammogram of solid cobalt-coated $Ni(OH)_2$ particles (Type A) on a glassy carbon electrode obtained at a scan rate of 20 mV s^{-1}. (a) E_{sw} = 600 mV; (b) E_{sw} = 550 mV.

probable that over-oxidation of nickel hydroxide has led to the formation of γ-phase (see discussion below).

Additional cycling of the nickel hydroxide electrode (continued from Fig. 1) using lower switching potentials (E_{sw}) is shown in Fig. 2. Cycles 21–30 (Fig. 2(a)) use a potential range of 0–600 mV and a decrease in E_{sw} by 50 mV clearly limits the amount of oxygen evolved (cf. Fig. 2(a) with Fig. 1(a or b)) and also slows the rate of capacity (and I_{ox}^{P}) loss. An almost constant capacity (negligible loss in I_{ox}^{P}) can be obtained with E_{sw} = 550 mV (Fig. 2(b)). This result demonstrates that cycling to a lower positive switching potential has the effect of reducing oxygen evolution and stabilizing the capacity of the active material.

To confirm that the loss in capacity observed in Figs. 1 and 2 is not due to the charging history of the electrode but is only dependant on the switching potential, a fresh electrode was subjected to the reverse series of experiments. Namely, for the initial 20 cycles the E_{sw} = 550 mV and is then increased to 600 mV for the next 20 cycles and finally to 650 mV for the last 10 cycles. Both the capacity and the current increase with each of the first 20 cycles at E_{sw} = 550 mV. The conditioning at these potentials is slow, as it is usually necessary to condition fully the electrode by applying slight overpotentials and evolving oxygen. The capacity reaches a maximum which is almost identical to that obtained previously (69 µA) at the 30th cycle (E_{sw} = 600 mV) and remains constant for a further 10 cycles. Increasing E_{sw} to 650 mV results in a loss of both peak current and capacity on cycling.

This set of experiments has confirmed that the use of positive electrode potentials in excess of 600 mV degrades the electrode and reduces the cycle-life of $Ni(OH)_2$. From the results, it appears that the potential at which detectable oxygen evolution begins corresponds to a potential of 560 mV. In considering further experiments, a safe operating potential limit of 550 mV versus Hg/HgO (1 M KOH) is adopted, at which minimal oxygen evolution will occur.

3.1.2. Effect of doping and cobalt coating on electrochemistry of nickel hydroxide and oxygen evolution reaction

The electrochemical behaviour of four types of commercial, battery-grade $Ni(OH)_2$ particles (Table 1) attached to GC electrodes was examined in order to investigate the effect of dopants and cobalt coating on the electrochemistry of $Ni(OH)_2$ in KOH. Fig. 3(a) shows the 10th cycle from a cyclic voltammetric experiment performed on each of the four types of $Ni(OH)_2$ over a sweep range of 0–600 mV. By design, the peak current is similar for each micro-particle electrode in order to enable direct comparison of the peak oxidation potential (E_{ox}^{P}) and, in particular, the onset potential of the oxygen evolution reaction (E_{OER}).

The shape and position of the oxidation process for the cobalt-coated $Ni(OH)_2$ hydroxide particles (Types A–C) show minor differences (Fig. 3(a)), whilst Type D $Ni(OH)_2$ (no cobalt coating) oxidizes at significantly more positive potentials, which results in a greater overlap with the OER process. Cobalt coating appears to shift the potential at which $Ni(OH)_2$ oxidizes to slightly more negative potentials without significantly influencing the onset potential of the OER. Types A and C have similar chemical compositions (Table 1) but Type A shows a small negative shift of the oxygen evolution onset (E_{OER}) potential and a sharpening of the $Ni(OH)_2$ oxidation wave (see Fig. 3(a)). The difference in peak shape is attributed to the greater crystallinity (lower FWHM, Table 1) of the Type A sample, which can influ-

Table 2
Peak potentials for the redox couple and oxygen evolution onset potential from cyclic voltammetry of nickel hydroxide micro-particles

$Ni(OH)_2$ Type	E_{red}^{P} (V)	E_{ox}^{P} (V)	E_{OER} (V)	ΔE^{P} (V)	$(E_{OER} - E_{ox}^{P})$ (V)
Type A	0.240	0.435	0.565	0.195	0.130
Type B	0.240	0.435	0.580	0.195	0.145
Type C	0.240	0.435	0.580	0.195	0.145
Type D	0.265	0.445	0.570	0.180	0.125

E_{ox}^{P}, nickel hydroxide oxidation peak potential; E_{red}^{P}, nickel oxy-hydroxide reduction peak potential; E_{OER}, onset potential for oxygen evolution (measured when current exceeds 10 µA above the nickel hydroxide process). Note: values given to nearest 5 mV.

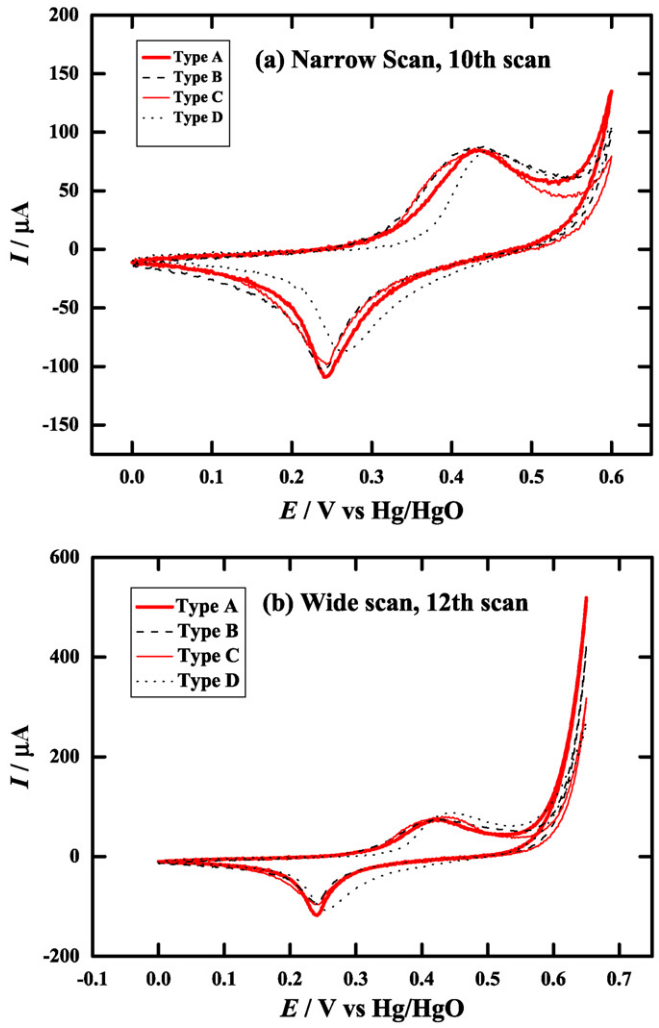

Fig. 3. Cyclic voltammograms of solid $Ni(OH)_2$ particles (Types A–D) on glassy carbon electrode obtained at scan rate of 20 mV s^{-1}. (a) 10th cycle (narrow range: E_{sw} = 600 mV); (b) 12th cycle (wide range: E_{sw} = 650 mV).

ence the kinetics of releasing a proton or charge compensator upon oxidation [42].

Table 2 summarises the oxidation and reduction peak potentials, determined from the micro-particle cyclic voltammetry, for the different grades of nickel hydroxide. As was evident in Fig. 3, Types A, B and C have similar oxidation (E^P_{ox}), reduction (E^P_{red}) and oxygen evolution onset (E_{OER}) potentials. The separation between the redox peaks, ΔE^P (or $[E^P_{ox} - E^P_{red}]$), is a combination of ohmic drop and the energetics of the ion insertion–expulsion reaction [43,44]. If ohmic drop is small (as would be the case for surface-adhered particles), the separation (ΔE^P) gives a measure of how difficult it is to insert and expel the counter ions [18,43,44]. This process appears to be more facile for the Type D material, with the other types of $Ni(OH)_2$ having similar peak-to-peak separations. A slight difference is also observed in the onset potential for oxygen evolution, see Table 2. The OER for Types B and C occur at slightly higher potentials than on the other materials (0.580 V). Type A has the lowest OER potential (0.565 V). Other workers have also observed small shifts in E_{OER} with the use of metal dopants and their effect was found to be strongly concentration dependent [23].

Determination of the E^P_{ox} and E_{OER} potentials for the Type D $Ni(OH)_2$ from cyclic voltammetry is more problematic due to the close overlap of the currents for the oxidation of the nickel hydroxide and the evolution of oxygen. An important parameter is the separation between the oxidation peak of the nickel hydroxide and the OER potential ($E_{OER} - E^P_O$), Table 2. The low ($E_{OER} - E^P_O$) value obtained for the Type D sample clearly demonstrates the advantage of using a cobalt coating and/or doped $Ni(OH)_2$ in batteries and is consistent with earlier studies [4–7,14,16,19–30]. According to the data in Table 2, the ($E_{OER} - E^P_O$) separation decreases in the order: Type B ~ Type C > Type A > Type D. Other research groups [23] have claimed larger potential shifts for thick films doped with Cd, Co and Zn, but these can be attributed to ohmic drop as non-doped layers of $Ni(OH)_2$ are less conducting. In these situations, an increase in ohmic drop has the effect of increasing the separation between the oxidation and reduction peak potentials and decreasing the peak height (whilst retaining the same charge). This is a classical response to increased ohmic drop [33] and highlights the low ohmic drop advantages of voltammetry on surface-adhered micro-particles.

Fig. 3(b) presents the 2nd cycle with E_{sw} = 650 mV for each of the electrodes previously cycled in Fig. 3(a), i.e., the 12th cycle overall. Here, the shape and size of the voltammetric wave for each type of nickel hydroxide is very similar and again the peak current for oxidation of Type D is closest to the onset of current of oxygen evolution. As previously observed, the current and capacity diminish with cycling for all four types of nickel hydroxide (A–D) when a relatively high switching potential, namely E_{sw} = 650 mV, is employed. This indicates that, at this potential, the active material is not significantly protected by the types and/or level of additives used in this study.

3.2. *Cyclic voltammetry of pasted nickel hydroxide positive electrodes*

Cyclic voltammetric scans for nickel hydroxide pasted electrodes on nickel current-collectors (after conditioning) are given in Fig. 4. The peak oxidation potentials for Types A–C occur at approximately 500 mV, with very similar peak shapes. The current in these voltammograms has been normalized to the mass of the pasted material. In this set of experiments, E^P_{ox} for Type B is the most removed from the E_{OER}. The separation between the oxidation and reduction peak (ΔE) is now much larger (of the order of 400–500 mV) and this can be largely attributed to uncompensated resistance (R_u). The most resistive sample is Type D (at 45 mA cm^{-2} constant-current cycling, ESR = 1.4 Ω cm^2 compared with 0.6–0.8 Ω cm^2 for Type A), but with a lower current (lower specific capacity) the IR_u contribution is smaller and so the peak separation is comparable with the other samples. Therefore, if information on the energetics of the proton expulsion/insertion process is required, voltammetry should be conducted on surface-adhered micro-particles where the effect of ohmic distortion is, if not negligible, at least greatly reduced.

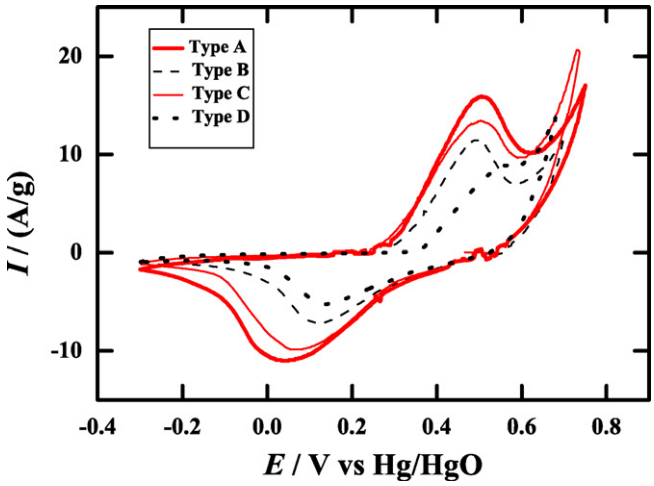

Fig. 4. Cyclic voltammetry of pasted nickel foil electrodes made from Types A–D with graphite and PVDF binder (currents have normalized to mass of pasted material). Obtained at a scan rate of 5 mV s^{-1} using an oversized metal-hydride electrode as counter electrode.

Type A, with the greatest specific capacity and absolute current, has the greatest peak separation, i.e., 470 mV, Fig. 4, Table 3. It is difficult to determine ($E_{OER} - E^{P}_{ox}$) from the cyclic voltammetry of Type D, which has a distorted oxidation wave that strongly overlaps and obscures the OER. For the pasted electrodes, the separation between the OER and the oxidation of nickel hydroxide ($E_{OER} - E^{P}_{ox}$) follows the sequence: Type B > Type A > Type C > Type D. This sequence differs from the results obtained using the surface-adhered $Ni(OH)_2$ micro-particles technique (see Section 3.1.2) and needs to be treated with caution due to the high ohmic distortion.

The results obtained from the cyclic voltammetry of Type D $Ni(OH)_2$ (which is the most resistive) using both the adhered micro-particles and pasted electrode techniques, is presented in Fig. 5. The data clearly illustrate the large amount of additional ohmic drop (>100 mV) for the oxidation process that is involved in the pasted electrode measurement and the ensuing error. It is also worth noting that the scan rate used for the micro-particles is faster than that for the pasted electrodes, viz., 20 mV s^{-1} versus 5 mV s^{-1}. This faster scan rate is easily achievable with micro-particles and still results in much less ohmic distortion. Additional inaccuracy in potential determinations also arises from the large oxidative currents generated by the pasted nickel hydroxide, which overwhelm the oxygen evolution current, until high overpotentials are reached.

Table 3
Peak potentials of the redox couple and oxygen evolution onset potential from the cyclic voltammetry of pasted nickel hydroxide electrodes

$Ni(OH)_2$ Type	E^{P}_{red} (V)	E^{P}_{ox} (V)	E_{OER} (V)	ΔE^{P} (V)	($E_{OER} - E^{P}_{ox}$) (V)
A	0.035	0.505	0.665	0.470	0.160
B	0.125	0.495	0.670	0.370	0.175
C	0.070	0.505	0.655	0.435	0.150
D	0.130	0.570	0.650	0.360	0.080

E_{OER} is measured 0.3 A above nickel hydroxide process. Note: values given to nearest 5 mV.

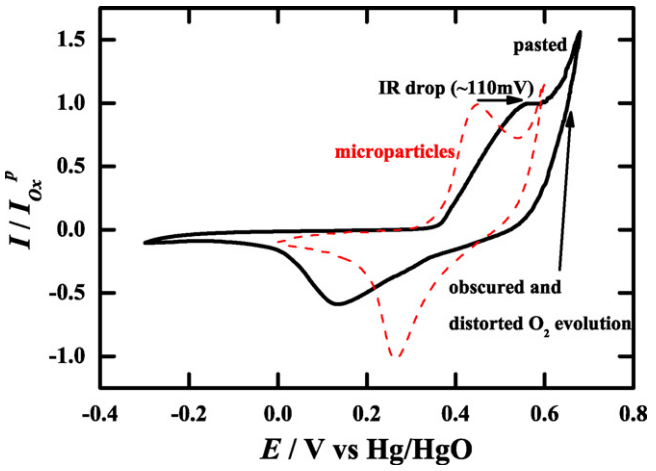

Fig. 5. Cyclic voltammetric comparison of adhered micro-particles (20 mV s^{-1}) and pasted (5 mV s^{-1}) Type D $Ni(OH)_2$. (Currents normalized to I^{P}_{ox}.)

3.3. Potential monitoring during constant-current charge–discharge cycling of positive nickel hydroxide electrode

To demonstrate the effect of excessive oxygen evolution on the capacity and the cycle-life of $Ni(OH)_2$ electrodes, and the value of monitoring the positive electrode potential, a series of pasted $Ni(OH)_2$ electrodes were subjected to a set of charge–discharge cycling experiments at relatively high currents. The cells, which comprised a pasted $Ni(OH)_2$ (Type A) positive electrode and an oversized metal-hydride negative electrode, were cycled in a three-electrode configuration. The cell and positive electrode potentials were monitored using a Hg/HgO reference electrode.

In one series of experiments, a 'severe' cycling profile was employed, in which the cells were charged at a constant current of 400 mA (equivalent to 18 mA cm^{-2} or ~23 C) for sufficient time to allow the active electrode material to achieve ~290 mAh g^{-1} (the theoretical capacity of nickel hydroxide). The cells were then discharged at 400 mA until the cell voltage fell below 0.8 V with a rest period of 1 min after each charge or discharge. As the cell potential is not limited, the positive electrode potential will most likely exceed 0.55 V versus Hg/HgO (the threshold at which the OER occurs on $Ni(OH)_2$) during charging. At these high currents, problems arising from oxygen evolution are exacerbated.

The cycling behaviour of a cell using the profile outlined above is given in Fig. 6(a). The capacity rises to 125 mAh g^{-1} (based on pasted material weight, which includes binder and graphite) and degrades rapidly within the first 50 cycles. This represents approximately 57% utilization of the $Ni(OH)_2$. An examination of the cell potential (Fig. 6(b)) shows that the potential clearly exceeds 1.5 V and reaches a plateau above 1.6 V. Correspondingly, the positive potential exceeds 550 mV for a significant period of time. Earlier cyclic voltammetry results, with both surface-adhered micro-particles and pasted $Ni(OH)_2$ electrodes, have demonstrated that at these high overpotentials the $Ni(OH)_2$ electrode will generate a large amount of oxygen, which results in degradation of positive electrode. The range

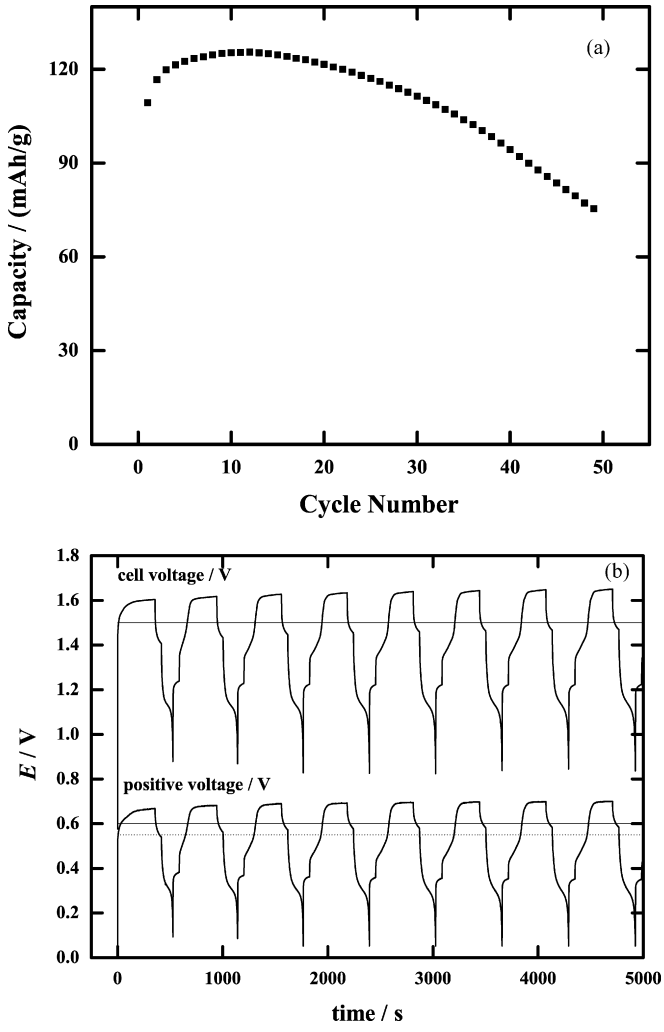

Fig. 6. Capacity of $Ni(OH)_2$ positive/oversized MH negative cell for 50 cycles. (a) Charging at 400-mA (equivalent to 290 mAh g^{-1}) and (b) discharging at 400 mA down to 0.8 V. Potential monitoring for first eight cycles.

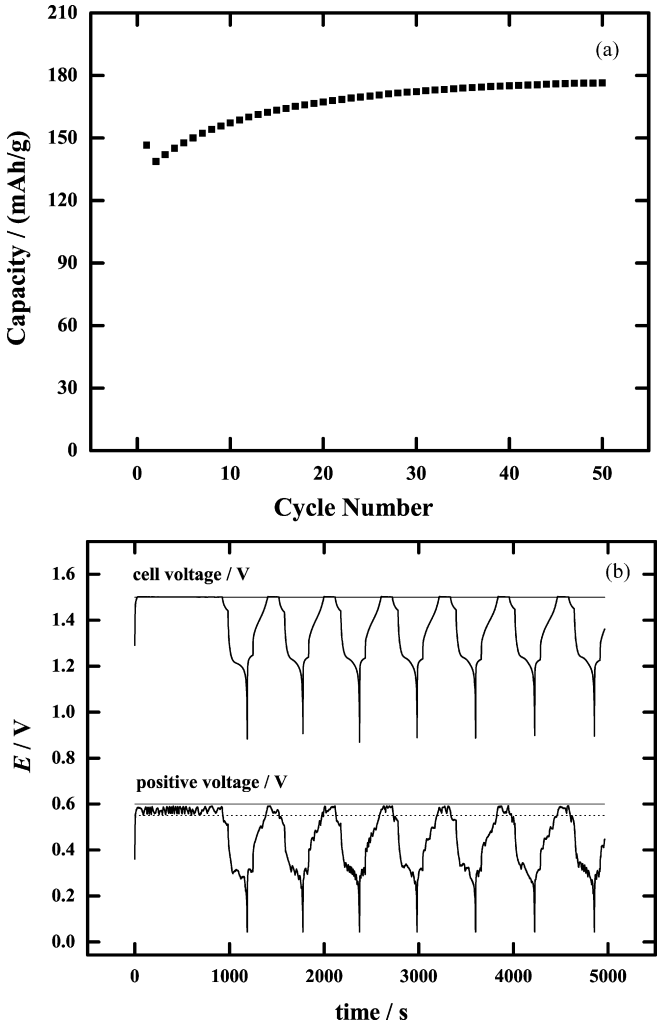

Fig. 7. Capacity of $Ni(OH)_2$ positive/oversized MH negative cell for 50 cycles. (a) Charging at 400 mA to 1.5 V then a 2-min constant voltage (1.5 V) step followed by discharge at 400 mA. (b) Potential monitoring for first seven cycles.

between which minimal oxygen evolution (550–600 mV) occurs is marked by a dotted line. Using the above charging profile, the positive electrode potential is clearly driven above its optimum potential range.

In a second, less-severe cycling profile, a cell was charged at constant current (400 mA or 18 mA cm^{-2}) to a cell potential limit of 1.5 V, followed by a constant voltage step at 1.5 V for 2 min. After a rest step of 1 min, the cell was discharged at constant current (400 mA) until the cell voltage fell below 0.8 V. The behaviour of a cell using the 1.5 V, voltage-limited, cycling profile is given in Fig. 7(a). The maximum capacity for this profile is higher (176 mAh g^{-1} based on pasted material weight; 81% utilization) than that observed without the 1.5 V limit (cf. Fig. 6(a)), and there is no capacity loss during the first 50 cycles (or subsequent 50 cycles). The data shown in Fig. 7(b) reveal that even though the cell voltage is limited, the potential of the positive electrode still exceeds 550 mV for significant periods of time, but does not exceed 600 mV. Whilst this less-severe profile (reduced oxygen evolution) results in a higher and more stable capacity for this cell, it is still anticipated that prolonged cycling will result in some degradation since, under this profile, the positive electrode is still pushed into the OER region. Consequently, a gentler charging profile would be required to maximize cycle-life, which would involve lower currents, different constant voltage times, and/or lower cell voltage limits. Lower currents will result in longer charging and discharging times, whilst a lower cell voltage limit may not realize full electrode capacity.

3.4. SEM and XRD examinations

Scanning electron micrographs of the cross-sections of selected electrodes before and after cycling are presented in Fig. 8. A typical micrograph of the pasted electrode before cycling (but after soaking in KOH) is given in Fig. 8(a). It is seen that the nickel hydroxide particles (light shade), which are typically 10 μm in diameter, are separated by the graphite binder mix. After cycling with no voltage limit (Fig. 8(b)), the $Ni(OH)_2$ particles are largely intact, but exhibit a fine structure of either another phase or, perhaps, the formation of micro-cracks within

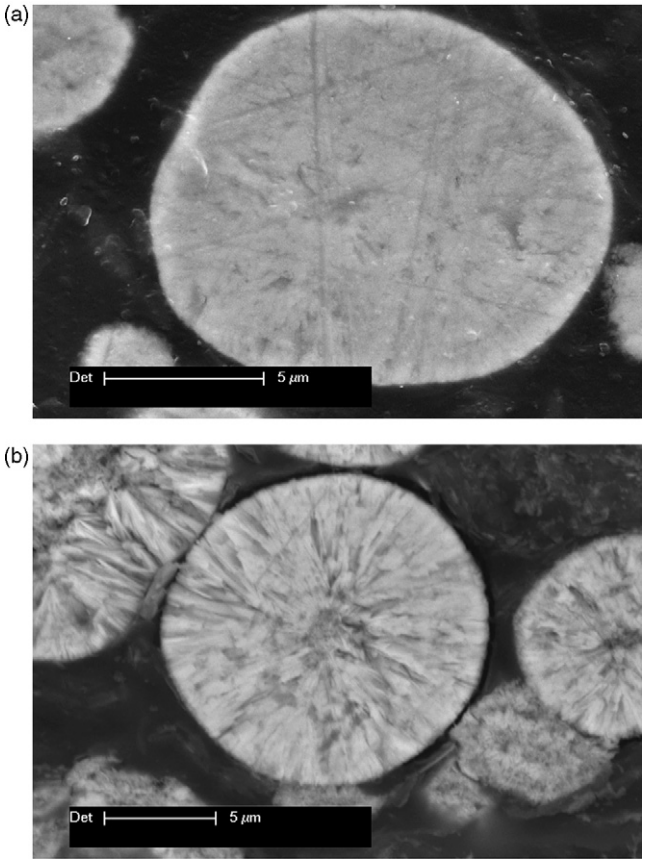

Fig. 8. Scanning electron micrograph of pasted electrode soaked in 7 M $KOH_{(aq)}$. (a) Before cycling and (b) after cycling with no voltage limit.

the crystals. There is also evidence of voids forming around the individual particles. These voids may develop as a result of the swelling and contraction of the particles upon cycling and may electrically isolate the particles and thus render them inactive. In the cycled electrode, potassium is detected within the nickel hydroxide particles, which is not the case within the uncycled (KOH soaked) electrode. This is consistent with the formation of the γ-phase of nickel oxy-hydroxide, which has a much larger interlayer spacing than β-nickel hydroxide and is known to intercalate larger ions such as potassium [14,45,46].

To confirm the presence of γ-NiOOH, XRD patterns were obtained for the as-received $Ni(OH)_2$, a $Ni(OH)_2$ electrode after ageing in KOH (before cycling), and a $Ni(OH)_2$ electrode that has been cycled at high currents (with no voltage limit) for around 100 cycles (resulting in 50% capacity loss). X-ray diffraction phase analysis confirms the as-received $Ni(OH)_2$ to be β-$Ni(OH)_2$. Ageing of the $Ni(OH)_2$ electrode in KOH (without cycling) only results in a slight shift in the *d*-spacing of one peak (from 4.64 to 4.66). Although this indicates a slight expansion in the interlayer spacing of the crystal structure, the material still retains all the other characteristic peaks of β-$Ni(OH)_2$. The XRD pattern of the cycled electrode showed only diffraction peaks corresponding to *d*-spacings of 7.01, 3.49 and 2.43. These peaks are consistent with the formation and presence of a predominant γ-phase [14].

The formation of γ-nickel oxy-hydroxide, by overcharging, is the likely cause of electrode deterioration in the high-current cycling tests. The material resulting from this less-ordered phase is mechanically unstable; it suffers from particle swelling/contraction during cycling that can give rise to particle fracturing and detachment. Inaccessible regions of nickel hydroxide are formed within the electrode and these become electrically isolated or inactive. The formation of γ-NiOOH is promoted by over-oxidation and by the OER. Additional tests that involved cycling of a cell with a 1.5 V limit resulted in little formation of the γ-phase and mostly β-phase remained as confirmed by XRD measurements.

4. Conclusions

Cyclic voltammetry has been performed on an array of nickel hydroxide micro-particles that are attached to a glassy carbon electrode. This allows accurate comparison of the potentials for nickel hydroxide oxidation (charging) and the onset of oxygen evolution. Using pasted electrodes, there is difficulty in determining E_{ox}^{P} and E_{OER} due to the occurrence of large ohmic distortions (>100 mV) and the ensuing error.

Monitoring the positive potential is essential for determining the relative degree of oxygen evolution and maintaining electrode capacity. By conducting cyclic voltammetry on $Ni(OH)_2$ micro-particles, it is demonstrated that oxygen evolution is significant above 550 mV (versus Hg/HgO) and, as such, this is a reasonably safe potential limit for cycling nickel hydroxide electrodes. At potentials above this limit, oxygen evolution becomes significant and results in capacity fading and decreased cycle-life. These two effects are linked to the formation of γ-NiOOH. By contrast, when the cell potential is limited to 1.5 V during galvanostatic cycling, less oxygen evolution occurs and improvements in capacity and cycle-life can be achieved.

Acknowledgements

Funding by the CSIRO *Energy Transformed Flagship* is gratefully acknowledged. Dr. Aaron Neufeld and Dr. Anthony Hollenkamp of CSIRO are thanked for guidance and valuable input. Warren Baldsing is also thanked for his assistance in the preparation of pasted electrodes.

References

[1] D. Linden, T.B. Reddy, Handbook of Batteries, third ed., McGraw-Hill, New York, 2002 (Chapter 26).
[2] E. Ahlberg, U. Palmqvist, N. Simic, R. Sjovall, J. Power Sources 85 (2000) 245–253.
[3] S. Deabate, F. Henn, Electrochim. Acta 50 (2005) 2823–2835.
[4] B. Liu, Z. Yunshi, H. Yuan, H.B. Yang, E.D. Yang, Int. J. Hydrogen Energy 25 (2000) 333–337.
[5] X.Y. Wang, J. Yan, Y.S. Zhang, H.T. Yuan, D.Y. Song, J. Appl. Electrochem. 28 (1998) 1377–1382.
[6] X.Y. Wang, J. Yan, Z. Zhou, J. Lin, H.T. Yuan, D.Y. Song, Y.S. Zhang, L.G. Zhu, Int. J. Hydrogen Energy 23 (1998) 873–878.
[7] Y.C. Ding, J.L. Yuan, Z.R. Chang, J. Power Sources 69 (1997) 47–54.
[8] A. Seghiouer, J. Chevalet, A. Barhoun, F. Lantelme, J. Electroanal. Chem. 442 (1998) 113–123.

[9] P. Oliva, J. Leonardi, J.F. Laurent, C. Delmas, J.J. Braconnier, M. Figlarz, F. Fievet, A. de Guibert, J. Power Sources 8 (1982) 229–255.
[10] A.B. Yuan, S.A. Cheng, J.Q. Zhang, C.N. Cao, J. Power Sources 77 (1999) 178–182.
[11] A.H. Zimmerman, P.K. Effa, J. Electrochem. Soc. 131 (1984) 709–713.
[12] H. Bode, J. Dehmelt, Electrochim. Acta 11 (1966) 1079.
[13] A.K. Shukla, S. Venugopalan, B. Hariprakash, J. Power Sources 100 (2001) 125–148.
[14] H. Chen, J.M. Wang, T. Pan, Y.L. Zhao, J.Q. Zhang, C.N. Cao, J. Power Sources 143 (2005) 243–255.
[15] Y.L. Zhao, J.M. Wang, H. Chen, T. Pan, J.Q. Zhang, C.N. Cao, Electrochim. Acta 50 (2004) 91–98.
[16] X.Y. Wang, H. Luo, H.P. Yang, P.J. Sebastian, S.A. Gamboa, Int. J. Hydrogen Energy 29 (2004) 967–972.
[17] B.L. Bourgault, B. Conway, Can. J. Chem. 37 (1959) 292.
[18] K.P. Ta, J. Newman, J. Electrochem. Soc. 146 (1999) 2769–2779.
[19] P.H.L. Notten, E. Verbitskiy, W.S. Kruijt, H.J. Bergveld, J. Electrochem. Soc. 152 (2005) A1423–A1433.
[20] M.Y. Wu, J.M. Wang, J.Q. Zhang, C.N. Cao, Acta Phys.-Chim. Sinica 21 (2005) 523–527.
[21] X. Mi, X.P. Gao, C.Y. Jiang, M.M. Geng, J. Yan, C.R. Wan, Electrochim. Acta 49 (2004) 3361–3366.
[22] H.S. Kim, T. Itoh, M. Nishizawa, M. Mohamedi, M. Umeda, I. Uchida, Int. J. Hydrogen Energy 27 (2002) 295–300.
[23] K. Provazi, M.J. Giz, L.H. Dall'antonia, S.I.C. De Torresi, J. Power Sources 102 (2001) 224–232.
[24] X.X. Yuan, Y.D. Wang, F. Zhang, J. Mater. Sci. Technol. 17 (2001) S119–S123.
[25] M. Oshitani, M. Watada, K. Shodai, M. Kodama, J. Electrochem. Soc. 148 (2001) A67–A73.
[26] B. Liu, X.Y. Wang, H.T. Yuan, Y.S. Zhang, D.Y. Song, Z.X. Zhou, J. Appl. Electrochem. 29 (1999) 855–860.
[27] X.Y. Wang, J. Yan, H.T. Yuan, Z. Zhou, D.Y. Song, Y.S. Zhang, L.G. Zhu, J. Power Sources 72 (1998) 221–225.
[28] W.H.H. Zhu, G.D. Zhang, D.J. Zhang, J.J. Ke, J. Chem. Technol. Biotechnol. 69 (1997) 121–129.
[29] A.A. Kamnev, Electrochim. Acta 41 (1996) 267–275.
[30] L. Indira, M. Dixit, P.V. Kamata, J. Power Sources 52 (1994) 93–97.
[31] S.I.C. De Torresi, K. Provazi, M. Malta, R.M. Torresi, J. Electrochem. Soc. 148 (2001) A1179–A1184.
[32] S.A. Cheng, A.B. Yan, H. Liu, J.Q. Zhang, C.N. Cao, J. Power Sources 76 (1998) 215–217.
[33] A.M. Bond, K.B. Oldham, G.A. Snook, Anal. Chem. 72 (2000) 3492–3496.
[34] G.A. Snook, A.M. Bond, S. Fletcher, J. Electroanal. Chem. 554 (2003) 157–165.
[35] G.A. Snook, Y. Cooney, T.E. Keyes, R.J. Forster, Langmuir 18 (2002) 9874–9881.
[36] A.M. Bond, R. Colton, P.J. Mahon, G.A. Snook, W.T. Tan, J. Phys. Chem. B 102 (1998) 1229–1234.
[37] G.A. Snook, N.D. Duffy, A.G. Pandolfo, ECS Transactions 2 (2007) 105–116.
[38] A. Palencsar, D.A. Scherson, Electrochem. Solid State 8 (2005) A328–A332.
[39] A. Palencsar, D.A. Scherson, Electrochem. Solid State 6 (2003) E1–E4.
[40] A. Palencsar, D.A. Scherson, Electrochem. Solid State 8 (2005) A622–A626.
[41] V.G. Kumar, N. Munichandraiah, P.V. Kamath, A.K. Shukla, J. Power Sources 56 (1995) 111–114.
[42] S. Deabate, F. Henn, S. Devautour, J.C. Giuntini, J. Electrochem. Soc. 150 (2003) J23–J31.
[43] A.M. Bond, S. Fletcher, P.G. Symons, Analyst 123 (1998) 1891–1904.
[44] A.M. Bond, S. Fletcher, F. Marken, S.J. Shaw, P.G. Symons, J. Chem. Soc. Faraday Trans. 92 (1996) 3925–3933.
[45] H. Arai, M. Tsuda, M. Hayashi, H. Ohtsuka, Y. Sakurai, Electrochim. Acta 50 (2005) 1821–1828.
[46] L. Guerloudemourgues, C. Delmas, J. Electrochem. Soc. 143 (1996) 561–566.